Article

Systematic Evaluation for the Impact of the Geological Conditions on the Adsorption Affinities of Calcite as an Adsorbent of Zn²⁺ Ions from Aqueous Solutions: Experimental and Theoretical Studies

Nourhan Nasser [1,2], Mohamed I. El-Sayed [1], Sarah I. Othman [3], Ahmed A. Allam [4], Ibrahim G. Al-Labadi [5], Mostafa R. Abukhadra [1,2,]* and Stefano Bellucci [6,]*

1   Geology Department, Faculty of Science, Beni-Suef University, Beni-Suef 65211, Egypt
2   Materials Technologies and Their Applications Lab, Geology Department, Faculty of Science, Beni-Suef University, Beni-Suef 65211, Egypt
3   Biology Department, College of Science, Princess Nourah Bint Abdulrahman University, Riyadh 11564, Saudi Arabia
4   Zoology Department, Faculty of Science, Beni-Suef University, Beni-Suef 65211, Egypt
5   Department of Environmental Analysis and Technologies, Institute of Environmental Sciences, Hungarian University of Agriculture and Life Sciences, Páter Károly u. 1, 2100 Gödöllő, Hungary
6   INFN—Laboratori Nazionali di Frascati, Via. E. Fermi 54, 00044 Frascati, Italy
*   Correspondence: abukhadra89@science.bsu.edu.eg (M.R.A.); stefano.bellucci@lnf.infn.it (S.B.)

Abstract: Three samples of calcite (calcite crystal (CA), calcite of limestone (L.CA), and metamorphosed calcite (marble) (M.CA)) were assessed as adsorbents of Zn (II) to consider the impact of the different geological conditions. The three samples exhibit remarkable changes in their Zn (II) retention capacities (Q_{sat} = 384.6 mg/g (CA), 274.5 mg/g (L.CA), and 512.6 mg/g (M.CA)). The retention systems of the three calcite samples were described on the basis of the suggested statistical physics-based equilibrium studies as well as the traditional kinetic and isotherm models. However, the M.CA samples exhibited the best retention capacity, the steric properties reflecting a higher active site density of CA ($N_{m\ (Zn)}$ = 113.46 mg/g) than both M.CA ($N_{m\ (Zn)}$ = 82.8 mg/g) and L.CA ($N_{m\ (Zn)}$ = 52.4 mg/g) at 323 K. This was assigned to the controlling effect of the sequestered numbers of Zn (II) per site on the surfaces of the calcite phase ($n_{(Zn)}$ = 3.39 (CA), 5.24 (L.CA), and 6.19 (M.CA)) in addition to the higher surface area and ion exchange of the metamorphosed and deformed M.CA. The previous $n_{(Zn)}$ values suggested the retention of Zn (II) by a multi-ionic mechanism in a vertical orientation. The Gaussian energies (8 to 16 KJ/mol) and retention energies (<40 KJ/mol) of Zn (II) by CA and L.CA suggested complex physical and weak chemical mechanisms involving ion exchange, hydrogen bonding, dipole bonding forces, electrostatic attractions, and van der Waals forces. The thermodynamic properties were illustrated on the basis of the internal energy, free enthalpy, and entropy functions, which validate the endothermic and spontaneous nature of the Zn (II) retention system by the three calcite samples.

Keywords: calcite; geological conditions; Zn (II) ions; retention; steric; energetic

1. Introduction

The water shortage, in addition to the increase in the concentrations of the common pollutants in the available water supplies, attracted the attention of interested researchers to develop effective management and remediation techniques [1,2]. The dissolved heavy metals in water were categorized as highly dangerous and toxic species of inorganic chemistry in the water supplies, which causes a serious threat to living organisms and humans [3]. Moreover, such metal ions exhibit bioaccumulation and non-biodegradability properties, which increase their toxicity effects [4–6]. The discharging of such toxic ions is

related to the industrial wastewater of mining, electroplating, battery manufacturing, and several industrial activities [7–9]. The presence of such metals at 50 μg/L concentration exhibits carcinogenic effects on the lungs, liver, or kidney for each 1 L of drinking water per day. In addition, the exposure of the human skin to the metal ions in regular rats at 0.0012 mg/kg/day is of significant damaging impact [10–12]. Among the recorded heavy metal ions, Zn (II) exhibits significant acute and chronic toxicity, and its existence in water causes significant health issues, including neurological signs, stomach-ache, vomiting, dizziness, diarrhea, loss of appetite, depression, profound neurological illnesses, and lethargy [10,13]. Therefore, the permissible concentration of Zn in drinking water was set to be no more than 3 mg/L (WHO, 2017) and lower than 1 mg/L, according to the recommended criteria of China Standards [10,14].

The adsorption of metal ions as Zn (II) by different natural and synthetic materials was evaluated in numerous studies as an effective, simple, and low-cost remediation technique [15,16]. However, it is still an attractive and hot research point, considering the qualification and nature of the used adsorbents as well as their reactivity and recyclability, in addition to other considerations, such as the kinetic rates, the preparation cost, the adsorption efficiency, the equilibrium behaviors, and the illustration of the mechanism either by the theoretical or the experimental studies [3,17,18]. The adsorption remediation techniques based on natural minerals and rocks are still the most effective technique based on the availability, escalation, environmental, and cost considerations [19–21]. However, the same minerals exhibit the same mineralogical properties in different geological environments; thus, it was reported that the geological conditions are of significant impacts on the crystallinity and physicochemical properties [22,23].

Calcite is one of the widely distributed minerals that exhibit an anhydrous crystalline structure of calcium carbonate ($CaCO_3$) composition [23,24]. It is a secondary mineral that is present in all types of rocks, and its precipitation is related to a wide range of aqueous solutions, such as hydrothermal solutions, marine water, and surface water [24–26]. It is a known industrial mineral that is used widely in the chemical, paper, glass, and pharmaceutical industries as well as water treatment processes [24,27]. Naturally, calcite can exist as a free mineral (calcite), a dominant component of rocks (limestone, marble, and carbonatites), and as the skeleton of numerous organisms (corals, coccolithophores, foraminifers, and pearl oysters) [24,28]. Calcite is the stable polymorph of calcium carbonate in the natural environment, and it shows remarkable variation in color, chemical composition, microstructural deformation, and crystallinity degree [25,26]. The varied forms of calcite reflect different geological conditions and tectonic effects, including the formation pressure and temperature, in addition to the post-formation effects, such as the weathering, compaction, dissolution, recrystallization, and the other digenesis conditions that strongly affect the morphology and crystal system of calcite mineral [25,28].

Structurally, calcite mineral exhibits a heterodesmic structure in which the formation atoms are bonded together with mixed covalent, ionic, and/or weak long-range interactions (such as hydrogen bonds and van der Waals ones) [29,30]. Calcite crystallizes like a composite structure, containing alternative layers of negatively charged carbonate ions held together by layers of calcium cations in which each Ca^{2+} ion exhibits octahedron coordination with six oxygen atoms from six different CO_2 [29,30]. Regarding the chemical reactivity of the calcite surface, the interaction between the dissolved ions along the calcite–water interfaces, including sorption and redox processes, occurs under non-equilibrium conditions [20,26,28]. Metal ions, such as Mg (II), Mn (II), and Fe (II), can be introduced into calcite, causing significant defects in the crystal structure, which have a great influence on the crystal structure, chemical reactivity, optical properties, mechanical properties, and electronic properties [20,27]. Therefore, the surface properties of calcite as adsorbent materials are still attractive research points both for environmental applications or reaction mechanisms and have not yet been covered by satisfactory studies. Therefore, the introduced study involved, for the first time, a deep investigation of the surface reactivity of different forms of calcite minerals that were formed at different geological conditions. This involves

highlighting the impact of the geological conditions on the properties of the calcite mineral as an adsorbent for Zn (II) ions by considering the theoretical assumptions of the advanced equilibrium models based on the statistical physics theory, which has not been investigated before. This involved investigation of the active sites' density, saturation capacity, number of adsorbed metals per site, adsorption energy, enthalpy, internal energy, and entropy.

2. Experimental Procedures

2.1. Materials and Characterization

Three natural calcite forms (calcite crystal (CA), calcite of limestone (L.CA), and metamorphosed calcite (marble) (M.CA)) were delivered from the Eastern desert rock units in Egypt. Zinc nitrate ($ZnNO_3$) (Sigma-Aldrich, Cairo, Egypt) of analytical grade was applied in the preparation of the stock solutions (1000 mg/L) to be applied during the adsorption studies. According to the observed XRD patterns, the three evaluated samples are highly crystalline and pure calcite without remarkable detection of impurities (Figure 1). However, there were observable differences in the crystal structure properties. The estimated microstrain percentages in the calcite crystals were 0.162% (CA), 0.163% (L.CA), and 0.235% (M.CA). This reflected the considerable deformation effect of the metamorphism process on the crystal lattice of calcite minerals. In addition, this was reflected in the estimated average crystallite size as the crystallite sizes of 9.32 nm, 9.31 nm, and 6.34 nm for CA, L.CA, and M.CA, respectively.
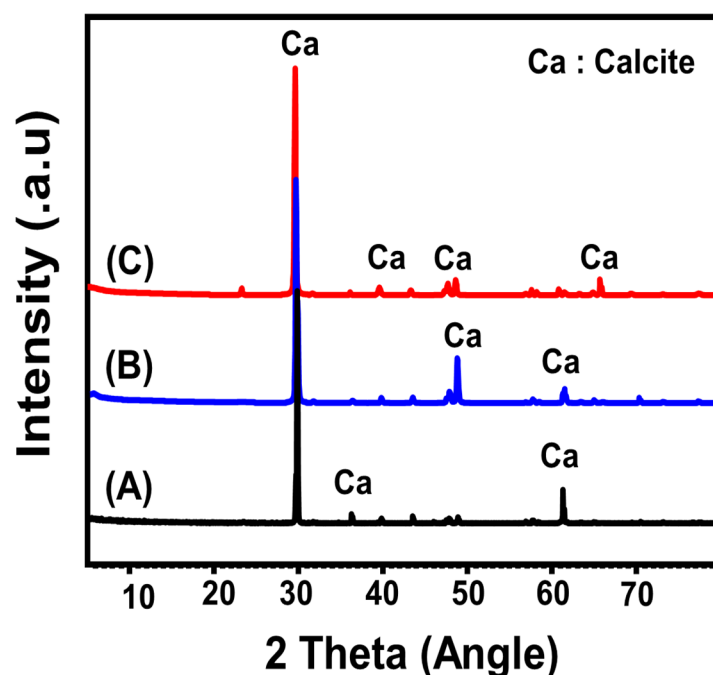

Figure 1. XRD patterns of the different evaluated calcite samples (A: CA, B: L.CA, and C: M.CA).

2.2. Batch Adsorption Studies

The retention tests of Zn (II) by the studied calcite samples were designed in batch form by considering main experimental factors, such as pH (2–7), the Zn (II) concentration (25 mg/L to 450 mg/L), and the adsorption duration (30 min to 900 min). The other experimental parameters were considered at certain values during the tests (0.2 g/L calcite dosage and 100 mL solution volume). The adsorption temperature during the equilibrium tests was evaluated at three values from 30 °C to 50 °C. The tests were completed in triplicate forms, and the measured values were inserted in their average values with standard deviations less than 3.4% (CA), 4.2% (L.CA), and 3.8% (M.CA). By the end of the tests or the equilibration period, the treated samples were separated from the calcite solids by filtration using Whitman filter paper (40 μm). After the filtration step, diluted nitric acid

was added carefully to the treated solutions to prevent the dissolved residual Zn (II) ions from precipitation on the walls of the utilized tubes. The residual concentrations of Zn (II) after completion of all the tests were measured by inductively coupled plasma mass spectrometry (Perkin Elmer) (ICP) in the existence of certified reference standard solution according to Merck Company (Germany) and the National Standard and Technology Institute (NIST). The measured concentrations were applied during the calculation of the Zn (II) retention capacities of the calcite samples according to Equation (1). The Q_e, C_o, C_e, V, and m symbols donate the calculated retention capacity in mg/g, initial Zn (II) concentrations (mg/L), the remaining Zn (II) concentration (mg/L), the volume of Zn (II)-polluted solution (mL), and calcite dosage (mg), respectively.

$$Q_{e\ (mg/g)} = \frac{(C_o - C_e)V}{m} \tag{1}$$

2.3. Theoretical Traditional and Advanced Equilibrium Studies

The retention systems of Zn (II) by the calcite samples were evaluated according to the theoretical assumptions of different kinetic, classic isotherm, and advanced equilibrium models, which were designed on the basis of the fundamentals of the statistical physics theory (Table S1). The inspection of the kinetic and classic equilibrium properties was accomplished according to the non-linear fitting degrees of the Zn (II) retention results, with the descriptive equations of the models considering the determined determination coefficient (R^2) (Equation (2)) and Chi-squared (χ^2) (Equation (3)). Regarding the non-linear fitting degrees of the Zn (II), retention results with the different illustrative equations of the assessed advanced equilibrium models were considered, according to the obtained values of the determination coefficient (R^2) and the recognized root mean square error (RMSE) (Equation (4)). The m', p, Qi_{cal}, and Qi_{exp} symbols in Equation (4) signify the Zn (II) retention results, retention parameters, theoretical Zn (II) retention capacity, and the experimentally determined Zn (II) retention capacity, respectively.

$$R^2 = 1 - \frac{\sum (Q_{e,\ exp} - Q_{e,\ cal})^2}{\sum (Q_{e,\ exp} - Q_{e,\ mean})^2} \tag{2}$$

$$\chi^2 = \sum \frac{(Q_{e,\ exp} - Q_{e,\ cal})^2}{Q_{e,\ cal}} \tag{3}$$

$$RMSE = \sqrt{\frac{\sum_{i=1}^{m} (Qi_{cal} - Qi_{exp})^2}{m' - p}} \tag{4}$$

3. Results and Discussion

3.1. Effect of pH

The experimental investigation of the impact of the pH of the solution on the actual affinities of the calcite surfaces to the Zn (II) ions was performed within the range from pH 2 to pH 7 at the highest value to avoid the expected precipitation of the metal ions as Zn $(OH)_2$. The main affecting variables were studied at 0.2 g/L for the calcite dosage, 240 min for the uptake duration, 100 mg/L for the Zn (II) concentration, 100 mL for the solution volume, and 303 K for the uptake temperature (Figure 2). The detected Zn (II) uptake results by the three types of calcite showed observable enhancement in terms of the adsorbed quantities of Zn (II) as the tested pH increased from pH 2 (14.7 mg/g (CA), 10.6 mg/g (L.CA), and 20.3 mg/g (M.CA)) to pH 7 (202.2 mg/g (CA), 145.2 mg/g (L.CA), and 215.7 mg/g (M.CA)) (Figure 2). These pH values demonstrated the suitability of the three calcite forms to be applied in the realistic decontamination of Zn (II) at neutral conditions, according to the recommended criteria of US EPA for the treatment of the industrial effluents (pH 6 to 9) [31]. This signified the impact of the pH on the solute dissociation, surface charges, and adsorption mechanism [32]. The speciation behavior of

Zn (II) validated the presence of its ions as Zn^{2+} cations up to pH 7, and converted them into positive hydrolytic form (Zn $(OH)^+$) from pH 7 to pH 11 [33]. Therefore, the neutral to alkaline conditions represented the best conditions to achieve significant electrostatic attractions with the Zn^{2+} ions, as the deprotonated calcite surfaces were highly saturated with the negatively charged hydroxyl radicals [32].
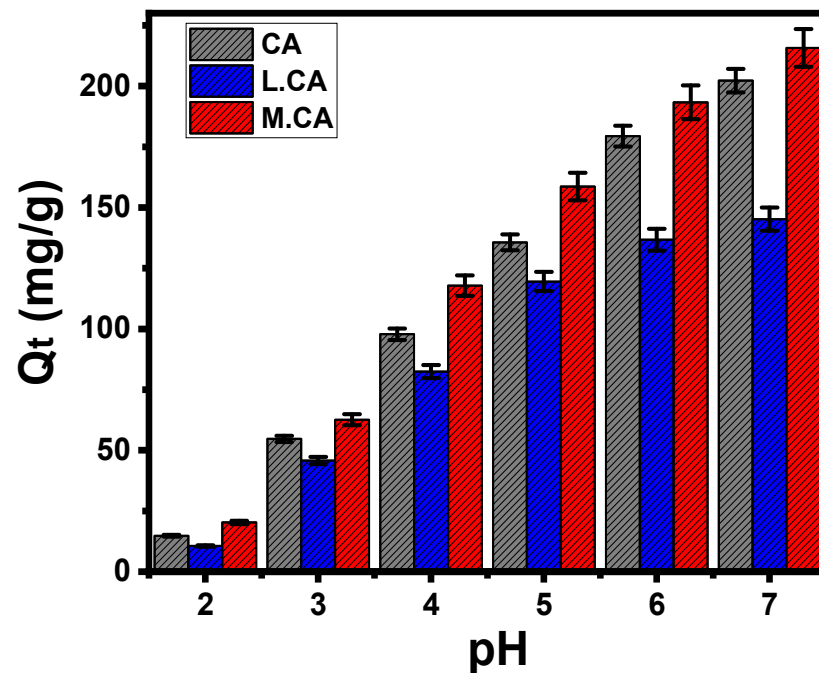

Figure 2. Effect of the solutions pH on the uptake of Zn (II) by the three calcite forms.

3.2. Kinetic Studies

3.2.1. Effect of Contact Time

The uptake properties of the three calcite forms (CA, L.CA, and M.CA), as evaluated adsorbents of Zn (II) in terms of the adsorption duration, were inspected from 30 min to 1140 min. The main affecting variables were studied at 0.2 g/L for the calcite dosage, pH 7, 100 mg/L for the Zn (II) concentration, 100 mL for the solution volume, and 303 K for the uptake temperature (Figure 3A). The obtained curves validated remarkable changes in the Zn (II) adsorption rates, with the studied duration forming two essential segments (Figure 3A). Within the initial Zn (II) uptake intervals, the processes showed high uptake rates with strong changes in the adsorbed Zn (II) quantities, as was signified by the steep slopes of the curves (Figure 3A). After 420 min, the actual rates declined significantly, and the calcite samples exhibited nearly fixed capacities, which normally identify the equilibrium states (Figure 3A). The determined Zn (II) equilibrium capacities of CA, L.CA, and M.CA were 211.5 mg/g, 203.2 mg/g, and 249.3 mg/g, respectively (Figure 3A). The saturation of the calcite surfaces with numerous active and free adsorption sites during the initial interactions between them and the Zn (II) ions resulted in effective adsorption of these ions at abrupt rates. With escalation of the duration, the Zn (II) ions occupied the free sites regularly, which reduced the availability and quantities of these sites, causing a remarkable drop in the adsorption rates. After a certain Zn (II) uptake interval, all the effective free sites were saturated and occupied with the metal ions, and no additional ions could be retained on the calcite surfaces, demonstrating their equilibrium states [16].
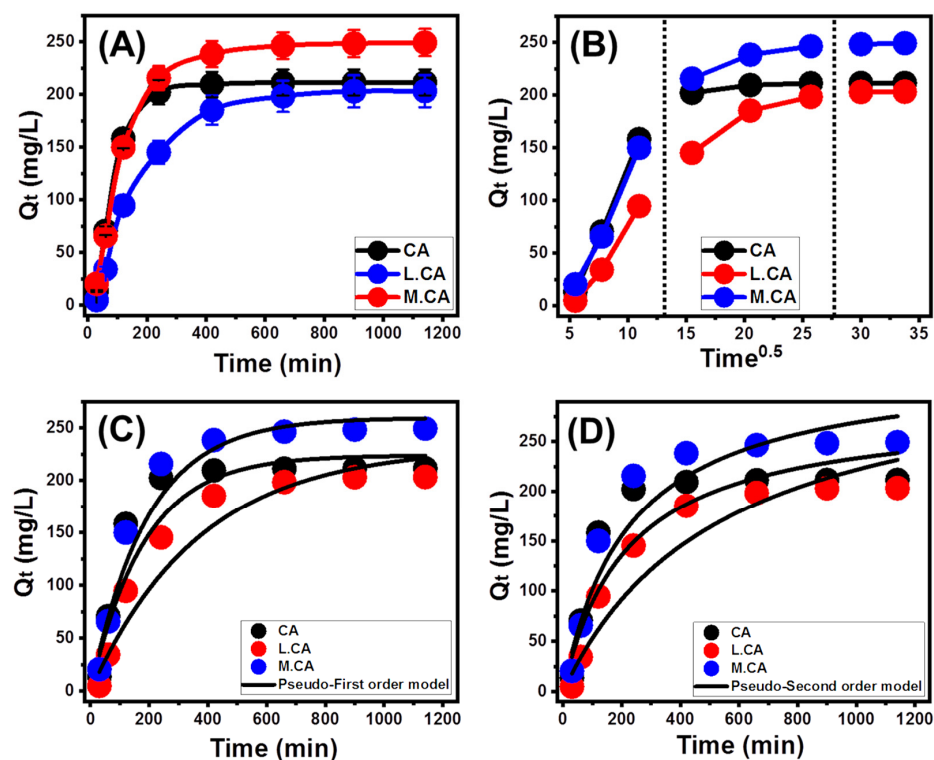
Figure 3. The impact of the contact time on the retention capacities of calcite phases for Zn (II) ions (**A**), the intra-particle diffusion curves of the Zn (II) retention results by the calcite phases (**B**), fitting of the Zn (II) retention results with the pseudo-first-order kinetic model (**C**), and fitting of the Zn (II) retention results with the pseudo-second-order kinetic model (**D**).

3.2.2. Intra-Particle Diffusion Behavior

The Zn (II) retention intra-particle diffusion curves utilizing the calcite phases demonstrated the presence of three remarkable segments with different slopes (Figure 3B). Moreover, these curves showed no observable intersections with the original points, demonstrating the cooperation of some parallel mechanisms in addition to the impact of the Zn (II) diffusion processes towards the calcite surface [34,35]. These properties suggested the presence of several processes, such as (A) external surface (border) adsorption, (B) intra-particle diffusion, and (C) saturation and equilibrium stage [36]. The reorganization of the starting segment within the initial Zn (II) retention duration suggested surficial and/or external retention of the ions, according to the availability of the free sites on the surface of calcite (Figure 3B) [19]. The detection of another segment that appeared during the intermediate intervals marked the occurrence of other types of retention mechanisms related to the intra-particle diffusion effect and the layered uptake processes (Figure 3B) [32,36]. During this stage, the dissolved Zn (II) diffused significantly into the interior structures of the calcite minerals [36,37]. The appearance of the third segment, mainly during the equilibration periods, reflected the saturation of all the present binding sites with the retained Zn (II) ions (Figure 3B) [3,35]. Moreover, this segment declared the retention of Zn (II) by molecular interaction and/or the interionic attraction reactions, and it resulted mainly in the formation of thick adsorbed layers of the metal ions [5].

3.2.3. Kinetic Modeling

The Zn (II) adsorption kinetics by the three calcite phases were assessed by considering the common theoretical basics of both pseudo-first-order (PFO) (Figure 3C) and pseudo-second-order (PSO) (Figure 3D) models. The determination of the fitting degrees of the occurred uptake reactions was considered according to the values of both the correlation coefficient (R^2) and Chi-squared (χ^2) (Table 1; Figure 3C,D). Considering these fitting parameters, the retention of Zn (II) by the three calcite phases occurred according to the kinetic behaviors of the PFO model rather than the kinetic assumption of the PSO model (Table 1). Therefore, the retention of Zn (II) by calcite might involve essentially physisorption processes, such as the impact of the electrostatic attractions [38,39]. This suggestion was supported by the detectable similarity between the actually measured retention capacities (211.5 mg/g (CA), 203.2 mg/g (L.CA), and 249.3 mg/g (M.CA)) and the theoretically obtained values (232 mg/g (CA), 223.8 mg/g (L.CA), and 259.6 mg/g (M.CA)) (Table 1). However, the observed high fitting with the PSO model demonstrated a considerable role for some chemical or even weak chemical reaction as assistant mechanisms during the physical retention of Zn (II) by calcite (electron exchange, surface complexation, and electron sharing) [35,38]. The physical and chemical retention mechanisms might have occurred on the surface of calcite, involving the formation of physically adsorbed Zn (II) ions layer above a layer of chemically adsorbed Zn (II) ions [40].

Table 1. The mathematical parameters of the studied kinetic models.

Kinetic Models			
	Model	**Parameters**	**Values**
CA	Pseudo-first-order	K_1 (1/min)	0.0027
		$Qe_{(Cal)}$ (mg/g)	232.06
		R^2	0.93
		X^2	5.6
	Pseudo-second-order	k_2 (mg/g min)	5.35×10^{-6}
		$Qe_{(Cal)}$ (mg/g)	342.5
		R^2	0.91
		X^2	7.2
L.CA	Pseudo-first-order	K_1 (1/min)	0.0054
		$Qe_{(Cal)}$ (mg/g)	223.8
		R^2	0.92
		X^2	5.4
	Pseudo-second-order	k_2 (mg/g min)	1.61×10^{-5}
		$Qe_{(Cal)}$ (mg/g)	284.2
		R^2	0.89
		X^2	8.3
M.CA	Pseudo-first-order	K_1 (1/min)	0.0051
		$Qe_{(Cal)}$ (mg/g)	259.6
		R^2	0.96
		X^2	4.2
	Pseudo-second-order	k_2 (mg/g min)	1.35×10^{-5}
		$Qe_{(Cal)}$ (mg/g)	329.2
		R^2	0.94
		X^2	6.7

3.3. Equilibrium Studies

3.3.1. Effect of Zn (II) Concentrations

The retention properties of Zn (II) by the three calcite phases in terms of the assessed starting concentration (50 mg/L to 450 mg/L) strongly signified the equilibrium behaviors as well as the actual maximum capacities. The main affecting variables were studied at 0.2 g/L for the calcite dosage, pH 7, 1140 min as contact time, and 100 mL for the solution volume by considering three values of the uptake temperature (303 K, 313 K, and 323 K) (Figure 4). The determined Zn (II) retention efficiencies by the three calcite phases in terms of the evaluated concentrations increased at remarkable rates (Figure 4A–C). The previous literature illustrates this behavior as a result of the strong increase in the driving forces of the Zn (II) ions as well as their diffusion speed with their increasing concentrations in the system. Therefore, the collision and interaction chances between such dissolved metals and the active sites on the calcite surfaces increased at significant rates, causing an enhancement in the actual retention capacities [41]. This could be detected within an experimental range from 50 mg/L to 200 mg/L for both CA and M.CA and up to 150 mg/L for L.CA (Figure 4A–C). These Zn (II) concentrations could be categorized as the equilibrium concentrations of the calcite adsorption systems, and all the tests conducted at concentrations other than these values demonstrated neglected or nearly fixed retention properties. Attending these stages reflects the complete saturation of the calcite phases with Zn (II) ions, i.e., their experimental maximum retention capacities. The maximum Zn (II) retention capacities of CA, L.CA, and M.CA at the best retention temperature (323 K) were 385 mg/g, 274.2 mg/g, and 511 mg/g, respectively (Figure 4A–C). The observable enhancement in the Zn (II) retention properties of the three calcite phases validated the endothermic properties of their adsorption systems.

3.3.2. Giles's Classification

The obtained Zn (II) retention curves of CA, L.CA, and M.CA in terms of the tested metal concentrations were classified according to the reported properties of Giles's classification for the isotherm curves. The obtained curves during the retention of Zn (II) by the calcite phases exhibited the properties of L-type isotherm curves [42] (Figure 4A–C). The reorganization of L-type curves reflected the strong effect of the present intermolecular attractive forces during the interaction between the Zn (II) ions and the reactive chemical groups of the calcite mineral (Figure 4A–C) [43]. The isotherm curves that exhibited L-type properties demonstrated the complete formation of adsorbed Zn (II) flat monolayers on the three calcite phases [44]. Moreover, this suggested the enrichment of the surfaces of the three calcite phases with numerous free and reactive chemical groups that exhibited remarkable affinity to adsorb the dissolved Zn (II) ions, even at low actual concentrations.

3.3.3. Classic Isotherm Models

The equilibrium properties of the Zn (II) retention processes using CA, L.CA, and M.CA were assessed by considering the reported assumptions of classic isotherm models, including Langmuir (Figure 4D–F), Freundlich (Figure 4G–I), and Dubinin–Radushkevich (D-R) (Figure 4J–L). The fitting degrees were obtained on the basis of the R^2 (determination coefficient) and χ^2 (Chi-squared) values of the non-linear fitting processes with the representative equations of the models (Table 2). The retention processes of Zn (II) by the three calcite phases followed the isotherm properties of the Langmuir Equation, as compared with the equilibrium behaviors of the Freundlich model. This behavior validated the monolayer retention of Zn (II) by the calcite phases in homogenous form based on active sites on their surfaces [3,19]. The theoretically obtained Q_{max} of Zn (II) values of CA, L.CA, and M.CA were 506.2 mg/g, 339.7 mg/g, and 727.5 mg/g, respectively, at the best-studied temperature (323 K) (Table 2).
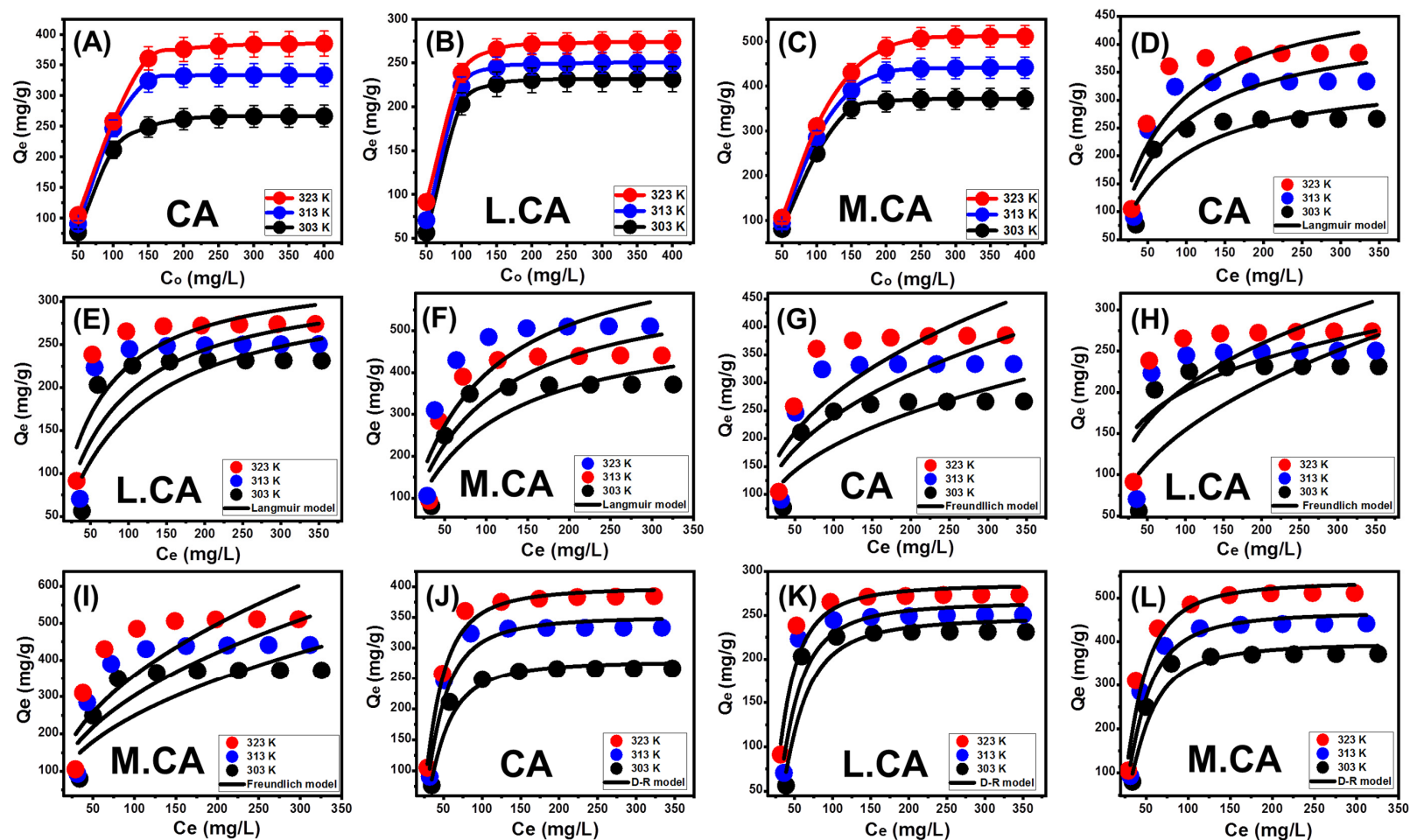
Figure 4. The impact of Zn (II) concentration on its retention by the three calcite phases (**A–C**), fitting of the Zn (II) retention results with Langmuir model (**D–F**), fitting of the Zn (II) retention results with Freundlich model (**G–I**), and fitting of the Zn (II) retention results with D-R model (**J–L**).
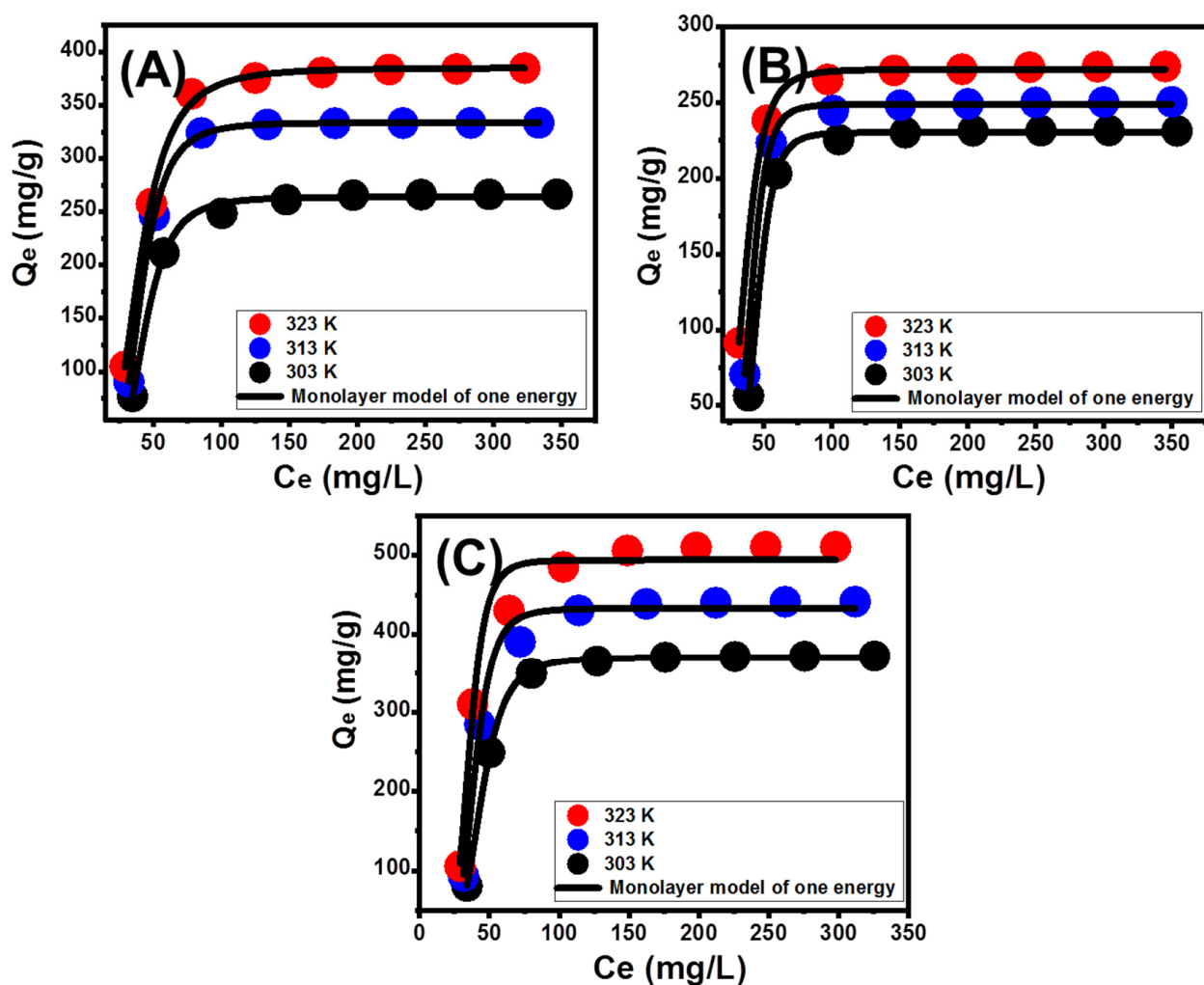
Table 2. The mathematical parameters of the studied classic isotherm models.

			303 K	313 K	323 K
CA	Langmuir model	Q_{max} (mg/g)	352.15	442.3	506.24
		b(L/mg)	0.0138	0.0146	0.0153
		R^2	0.84	0.822	0.86
		X^2	5.7	6.5	4.8
	Freundlich model	1/n	0.39	0.39	0.39
		k_F (mg/g)	30.46	38.39	44.45
		R^2	0.73	0.71	0.75
		X^2	6.8	7.4	6.2
	D-R model	β (mol²/KJ²)	0.0055	0.0049	0.0042
		Q_m (mg/g)	278.2	351.7	399.23
		R^2	0.97.	0.97	0.97
		X^2	1.03	1.62	1.62
		E (KJ/mol)	9.46	10.1	10.7
L.CA	Langmuir model	Q_{max} (mg/g)	323.27	329.07	339.7
		b(L/mg)	0.01	0.014	0.019
		R^2	0.81	0.80	0.83
		X^2	6.77	6.21	5.7
	Freundlich model	1/n	0.44	0.24	0.32
		k_F (mg/g)	20.23	65.9	45.6
		R^2	0.67	0.51	0.68
		X^2	8.78	9.2	8.5
	D-R model	β (mol²/KJ²)	0.0073	0.0062	0.0055
		Q_m (mg/g)	247.69	265.09	285.46
		R^2	0.93	0.92	0.95
		X^2	3.9	3.55	1.75
		E (KJ/mol)	8.27	8.98	9.5
M.CA	Langmuir model	Q_{max} (mg/g)	535.3	630.35	727.5
		b(L/mg)	0.01	0.011	0.012
		R^2	0.81	0.81	0.82
		X^2	7.8	7.5	6.7
	Freundlich model	1/n	0.47	0.47	0.47
		k_F (mg/g)	27.98	34.4	40.4
		R^2	0.71	0.72	0.73
		X^2	9.2	9.5	8.8
	D-R model	β (mol²/KJ²)	0.0063	0.0053	0.0045
		Q_m (mg/g)	396.5	467.4	537
		R^2	0.96	0.96	0.96
		X^2	3.01	4.01	4.58
		E (KJ/mol)	8.16	9.7	10.5

Regarding the assessed D-R model, the parameters of this model strongly signified the apparent energetic heterogeneity of evaluated adsorption systems that exhibited either homogenous or heterogeneous surface properties [45]. Moreover, the values of Gaussian energy (E), as theoretical parameters of this model, strongly signified the nature of the occurred retention reaction—either physical processes or chemical processes. Detecting the Gaussian energy at values less than 8 KJ/mol reflects the operation of a strong physical retention mechanism, within the range of 8 to 16 KJ/mol signifies the operation of weak chemisorption processes involving ion exchange mechanisms, and higher than 16 KJ/mol signifies strong chemisorption mechanisms [3,45]. Therefore, the determined E values of the Zn (II) retention processes by CA (9.46–10.7 kJ/mol), L.CA (8.27–9.5 kJ/mol), and M.CA (8.16–10. 5 kJ/mol) revealed weak chemisorption retention of the Zn (II) ions (Table 2). Moreover, these values were within the signified range of zeolite ion exchange reactions (0.6 kJ/mol to 25 kJ/mol) [35]. Such equilibrium results, in addition to the kinetic finding, suggested cooperation of physical and chemical processes during the retention of Zn (II) by the three calcite phases.

3.3.4. Advanced Isotherm Models

The equilibrium models based on the isotherm assumptions of the statistical physics theory have been evaluated as advanced models that can provide more information about the retention mechanism of Zn (II) by calcite in terms of the adsorbate/adsorbent interaction. A monolayer model of one energy site was selected to represent the retention systems of the three calcite phases on the basis of the recognized fitting degrees (Figure 5A–C). The fitting processes were completed by considering the Levenberg–Marquardt iterating algorithm as a function of multivariable nonlinear regression. The mathematical parameters of the model were obtained in terms of the steric parameters (number of adsorbed Zn (II) (n), occupied site density (N_m), and saturation adsorption capacity of calcite (Q_{sat})) and energetic parameters (retention energy (ΔE), internal energy (E_{int}), free enthalpy (G), and entropy (S_a)) (Table 3).

Figure 5. Fitting of the Zn (II) retention results by CA (**A**), L.CA (**B**), and M.CA (**C**) with advanced monolayer isotherm model of one energy site.

Table 3. The mathematical parameters of the studied advanced isotherm model.

		303 K	313 K	323 K
Advanced Isotherm Model				
Steric and Energetic Parameters				
CA	R^2	0.998	0.999	0.999
	X^2	0.09	0.002	0.06
	n	4.35	4.31	3.39
	N_m (mg/g)	61.5	76.17	113.46
	Q_{sat} (mg/g)	267.5	333.62	384.62
	$C_{1/2}$ (mg/L)	42.43	39.95	38.83
	ΔE (kJ/mol)	10.49	10.99	11.42
L.CA	R^2	0.999	0.999	0.999
	X^2	0.019	0.016	0.016
	n	7.32	7.12	5.247
	N_m (mg/g)	31.7	35.3	52.4
	Q_{sat} (mg/g)	232.0	251.3	274.5
	$C_{1/2}$ (mg/L)	45.15	40.86	36.11
	ΔE (kJ/mol)	10.33	10.93	11.61
M.CA	R^2	0.999	0.995	0.998
	X^2	0.021	0.62	1.76
	n	5.07	5.8	6.19
	N_m (mg/g)	73.8	76.78	82.8
	Q_{sat} (mg/g)	374.2	445.3	512.5
	$C_{1/2}$ (mg/L)	43.56	38.94	35.4
	ΔE (kJ/mol)	10.4	11.1	11.67

Steric Properties

Number of Adsorbed Zn (II) ($n_{(Zn)}$) per Site

The determined values of $n_{(Zn)}$ parameters strongly signified the orientation of the adsorbed Zn (II) ions in addition to the expected retention mechanisms in terms of the multi-docking or multi-interactions processes. Recognition of the $n_{(Zn)}$ parameter at values lower than unity ($n < 1$) reflected the horizontal orientation of the adsorbed Zn (II) ions by the multi-docking process (one Zn (II) ion adsorbed by more than one active site). Conversely, the estimation of the $n_{(Zn)}$ parameter at values greater than unity ($n > 1$) signified the vertical orientation of the adsorbed Zn (II) ions by multi-ionic processes (each site can adsorb more than one Zn (II) ions) [3,46,47]. The obtained values of $n_{(Zn)}$ during the retention processes by CA ($n = 3.39$–4.35), L.CA ($n = 5.2$–7.3), and M.CA ($n = 5.07$–6.19) were greater than 1 (Figure 6A–C; Table 3). This validated the suitability of the active sites on the surfaces of CA, L.CA, and M.CA to adsorb up to five, eight, and seven Zn (II) ions, respectively. Such changes in the efficiencies of the active sites of the three calcite phases reflected a significant impact on the surface reactivity of calcite as a function of the crystallinity degrees or the present impurities. Moreover, these values revealed the retention of the Zn (II) ions by multi-ionic mechanisms and the orientation of these ions in a vertical form [41].
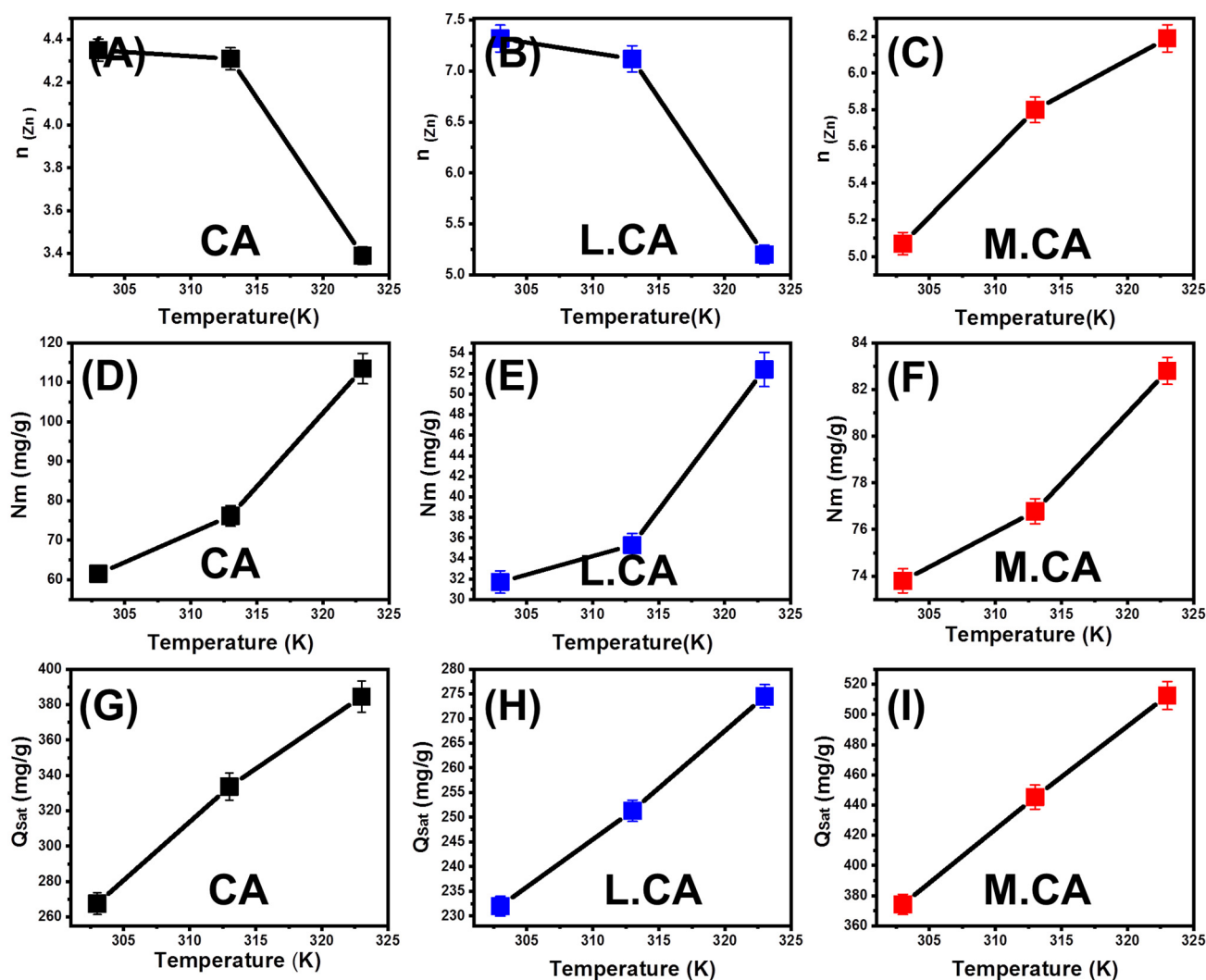
Figure 6. The change in the number of adsorbed Zn (II) ions per active site with temperature (**A**–**C**), the change in occupied active sites density of the calcite phases with temperature (**D**–**F**), and the change in the saturation retention capacities of the three calcite phases with temperature (**G**–**I**).

Regarding the impact of temperature of the adsorbed Zn (II) ions by each active site, the estimated $n_{(Zn)}$ values by both CA and L.CA declined at considerable rates with the tested retention temperature from 303 K to 323 K (Figure 6A,B; Table 3). This might be assigned to the declination in the aggregation properties of Zn (II) ions and their abrupt retention at high percentages by the present sites on the surfaces of CA and L.CA, especially at the high-temperature conditions [41]. Other studies suggested a significant effect of the temperature in inducing the diffusion of the Zn (II) to be in contact with more active sites or their substitution within the calcite structure [3]. The metamorphosed calcite (marble (M.CA)), as per the detected $n_{(Zn)}$ values, increased at significant rates in terms of the assessed temperature from 303 k to 323 K (Figure 6C; Table 3). This suggested thermal or energetic activation of the M.CA surface during the retention of Zn (II) ions, causing an enhancement in the aggregation behavior of the Zn (II) [2,48]. Moreover, this demonstrated a slight enhancement impact for the temperature on the substitution of Ca^{2+} on the structure of metamorphosed calcite by Zn^{2+}, as compared with CA and L.CA.

Occupied Active Site Density ($N_{m\ (Zn)}$)

The Zn (II) occupied active site density ($N_{m\ (Zn)}$) validated the quantities of the present receptors on the surface and structure of calcite during the performed retention reactions. The recognized $N_{m\ (Zn)}$ values during the retention of Zn (II) by CA were 61.5 mg/g

(303 K), 76.17 mg/g (313 K), and 113.46 mg/g (323 K) (Figure 6D; Table 3). The estimated values by L.CA were 31.7 mg/g (303 K), 35.3 mg/g (313 K), and 52.4 mg/g (323 K) (Figure 6E; Table 3), and by M.CA, the estimated values were 73.8 mg/g (303 K), 76.7 mg/g (313 K), and 82.8 mg/g (323 K) (Figure 6F; Table 3). The presented values declared the enrichment of both CA and M.CA with higher quantities of active sites, as compared with L.CA, which might be related to predicting lower reactive silica impurities within the limestone calcite (L.CA). In addition, the higher $N_{m\,(Zn)}$ values of CA, compared with M.CA, at the high-temperature conditions (323 K) might be related to the expected enhancement effect of temperature on the exchange of Ca^{2+} by Zn^{2+} on the structure of pure calcite (CA), as compared with metamorphosed and recrystallized calcite (M.CA). Regarding the impact of the retention temperature on the quantities of the active sites, the three calcite phases exhibited increment in the $N_{m\,(Zn)}$ values in terms of the retention temperature from 303 K to 323 K. This behavior was assigned to the enhancement impact of temperature on the substitution efficiency of Ca^{2+} by Zn^{2+}, providing additional active receptors in addition to its effect in inducing the diffusion of the Zn (II) ions to be in contact with internal structures of calcite grains [1,49].

Adsorption Capacity at the Saturation State the Calcite Phases ($Q_{sat\,(Zn)}$)

The estimated theoretical values of $Q_{sat\,(Zn)}$ significantly reflected the maximum Zn (II) retention capacities of CA, L.CA, and M.CA. The recognized $Q_{sat\,(Zn)}$ values by CA were 267.5 mg/g (303 K), 333.6 mg/g (313 K), and 384.6 mg/g (323 K) (Figure 6G; Table 3). The estimated values by L.CA were 232 mg/g (303 K), 251.3 mg/g (313 K), and 274.5 mg/g (323 K) (Figure 6H; Table 3), and by M.CA, the estimated values were 374.2 mg/g (303 K), 445.3 mg/g (313 K), and 512.6 mg/g (323 K) (Figure 6I; Table 3). The trends of the previous results validated enhancement effect for the temperature, reflecting the endothermic properties of the Zn (II) retention reactions by the calcite minerals at the different geological conditions. The obtained trends for CA and L.CA were in agreement with the trends of $N_{m\,(Zn)}$ rather than $n_{(Zn)}$, i.e., their efficiencies depended mainly on the present active sites. However, the observed trend of $Q_{sat\,(Zn)}$ by M.CA was in agreement with both $N_{m\,(Zn)}$ and $n_{(Zn)}$, i.e., its adsorption Zn (II) retention capacity was controlled by both the present site and the capacity of each site. This might be illustrated by the higher experimental capacity of M.CA, as compared with both L.CA and CA. Additionally, the metamorphosed and deformation properties of M.CA are normally associated with brittle failure and cataclasis effects, which reduce its crystal size and, in turn, induce its grindability and surface area, and this was in agreement with the XRD findings [50–52].

Moreover, the obtained adsorption capacities values demonstrated higher adsorption properties of the investigated calcite samples, as compared with several studied expensive adsorbents, especially the metamorphosed calcite (M.CA) (Table 4). This signified the technical value of natural calcite as an effective, available, and low-cost adsorbent material that can be applied effectively in the remediation of the water resources from metal ions.

Table 4. Comparison of the studied calcite phases and other adsorbents in literature.

Adsorbents	Q_{max}	References
ECSDNH	160.19	[53]
Kaolinite nanotubes (KNTs)	204.8	[54]
Biochar–Alginate composite	120	[55]
Amino–$Fe_3O_4@SiO_2$	169.5	[56]
CoS HNCs	151.51	[57]
nHAP	285	[58]
HAP/pectin	333.3	[59]
CMC-CAP	141.1	[60]
CA	384.6	This study
L.CA	274.5	This study
M.CA	512.6	This study

Energetic Properties

Retention Energy

The retention energies of Zn (II) by CA, L.CA, and M.CA (ΔE) can interpret the operated retention mechanism (physical or chemical). For chemical adsorption, $\Delta E > 80$ kJ/mol, while for physical adsorption, $\Delta E \leq 40$ kJ/mol. The physical adsorption may have occurred due to coordination exchange ($\Delta E = 40$ kJ/mol), hydrogen bonding ($\Delta E < 30$ kJ/mol), dipole forces ($\Delta E = 2$ to 29 kJ/mol), van der Waals forces ($\Delta E = 4$ to 10 kJ/mol), or hydrophobic bonds ($\Delta E = 5$ kJ/mol). The adsorption energy (ΔE) can be calculated theoretically from Equation (5) by considering the values of the other variables, such as the gas constant ($R = 0.008314$ kJ/mol.K), absolute temperature (T), solubility values of the adsorbates (S), and the concentrations of the adsorbates at the half-saturation states of the calcite phases [50,51].

$$\Delta E = RT \, \ln\left(\frac{S}{C}\right) \tag{5}$$

The calculated ΔE values of the occurred Zn (II) retention reactions by CA were 10.49 kJ/mol (303 K), 10.99 kJ/mol (313 K), and 11.42 kJ/mol (323 K) (Table 3). The estimated values for the retention processes by L.CA were 10.33 kJ/mol (303 K), 10.93 kJ/mol (313 K), and 11.6 kJ/mol (323 K), while the recognized values by M.CA were 10.4 kJ/mol (303 K), 11.1 kJ/mol (313 K), and 11.67 kJ/mol (323 K) (Table 3). These values indicated the dominance of the physical processes during the retention of Zn (II) by the three calcite phases (dipole bond forces, van der Waals forces, and hydrogen bonding). Furthermore, the positive signs of ΔE values for the occurred retention reactions by CA, L.CA, and M.CA validated the endothermic behaviors of these processes.

Thermodynamic Functions

Entropy

The entropy (S_a) properties of the occurred Zn (II) retention reactions by CA, L.CA, and M.CA displayed the disorder and order properties of their surfaces at the different concentrations of the adsorbates and different retention temperature. The values of S_a can be calculated according to Equation (6) using the previously obtained values of $Nm_{(Zn)}$ and $n_{(Zn)}$, and $C_{1/2}$ (concentration at half-saturation) parameters [51].

$$\frac{S_a}{K_B} = Nm\left\{ \ln\left(1 + \left(\frac{C}{C_{1/2}}\right)^n\right) - n\left(\frac{C}{C_{1/2}}\right)^n \frac{\ln\left(\frac{C}{C_{1/2}}\right)}{1 + \left(\frac{C}{C_{1/2}}\right)^n} \right\} \tag{6}$$

The calculated values of S_a for the retention of Zn (II) by CA, L.CA, and M.CA decreased at considerable rates in the presence of high concentrations of them in the solutions (Figure 7A–C). Therefore, the disorder properties of the three calcite phases decreased significantly with the assessed high Zn (II) concentrations. In addition, this signified the expected dock of Zn (II) on the free retention sites of the calcite phases at the low tested concentrations [50,51]. The equilibrium Zn (II) concentrations that corresponded to the maxima values of S_a by CA were 50.12 mg/L (303 K), 43.6 mg/L (313 K), and 37.9 mg/L (323 K), while the estimated values of L.CA were 54.6 mg/L (303 K), 47.3 mg/L (313 K), and 41.8 mg/L (323 K) (Figure 7A,B). The estimated values for M.CA were 38.7 mg/L (303 K), 35.8 mg/L (313 K), and 31.7 mg/L (323 K) (Figure 7C). The previously mentioned Zn (II) concentrations were close to their concentrations at the half-saturation states of CA as well as L.CA and M.CA. Therefore, no additional Zn (II) could be docked on the active sites of the used calcite phases. Moreover, the steady declines in the S_a values revealed a remarkable decrease in both freedom degrees and diffusion properties of these ions in addition to the strong depletion in the free adsorption sites [52].
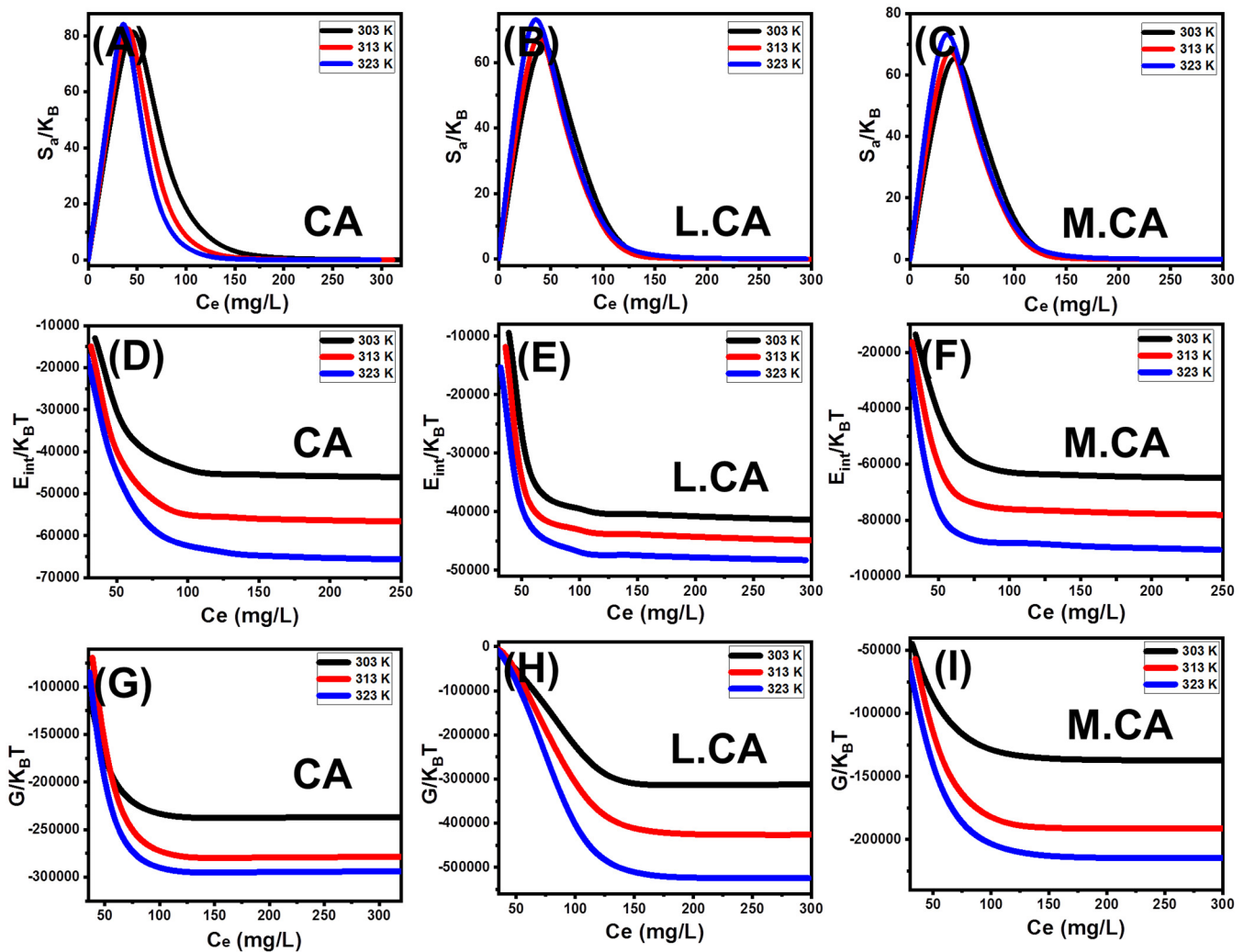
Figure 7. The change in the entropy properties of the Zn (II) retention processes by the calcite samples (**A–C**), the change in the internal energy properties of the Zn (II) retention processes by the calcite samples (**D–F**), and the change in the free enthalpy properties of the Zn (II) retention processes by the calcite samples (**G–I**).

Internal Energy and Free Enthalpy

The internal energy (E_{int}) and free enthalpy (G) properties of Zn (II) retention processes by CA, L.CA, and M.CA were evaluated on the basis of the calculated values from Equations (7) and (8), respectively, using the previously obtained values of $N_{m\,(Zn)}$ and $n_{(Zn)}$ and $C_{1/2}$ (concentration at half-saturation) parameters in addition to the value of translation partition (Z_v) [48].

$$\frac{E_{int}}{K_B T} = n\,N_m \left[\left(\frac{\left(\frac{C}{C_{1/2}}\right)^n ln\left(\frac{C}{Z_v}\right)}{1 + \left(\frac{C}{C_{1/2}}\right)^n} \right) - \left(\frac{n\,\ln\left(\frac{C}{C_{1/2}}\right)\left(\frac{C}{C_{1/2}}\right)^n}{1 + \left(\frac{C}{C_{1/2}}\right)^n} \right) \right] \tag{7}$$

$$\frac{G}{K_B T} = n\,N_m \frac{\ln\left(\frac{C}{Z_v}\right)}{1 + \left(\frac{C_{1/2}}{C}\right)^n} \tag{8}$$

The recognized E_{int} values of Zn (II) retention reaction by CA, L.CA, and M.CA exhibited negative signs and increased regularly with the temperature from 303 K to 323 K (Figure 7D–F). On the basis of these results and behaviors, the CA as well as L.CA and

M.CA retention systems of Zn (II) were characterized by spontaneous and endothermic behaviors (Figure 7D–F). The recognized free enthalpy values (G) demonstrated the same behaviors and findings (Figure 7G–I). The negative signs of G values, as well as the observed increase in these values with the adsorption temperature, confirmed the spontaneous and endothermic properties of the studied retention systems of Zn (II) by the three calcite phases (Figure 7G–I).

4. Conclusions

The retention properties of pure calcite crystal (CA), calcite of limestone (L.CA), and metamorphosed calcite (marble) (M.CA)) were evaluated as adsorbents for Zn (II). The metamorphosed sample (M.CA) exhibited a higher retention capacity (512.6 mg/g) than both CA (384.6 mg/g) and L.CA (274.5 mg/g). However, the CA sample exhibited the best active site density (N_m (Zn) = 113.46 mg/g); as compared with L.CA (N_m (Zn) = 52.4 mg/g) and M.CA (N_m (Zn) = 82.8 mg/g), it exhibited a lower number of adsorbed Zn (II) per site (n (Zn) = 3.39) than M.CA (n (Zn) = 6.19). This, in addition to the deformation properties of M.CA, explains its higher retention capacity than that of CA, and the presence of silica impurities explains the low adsorption capacity of L.CA. The three samples exhibited Gaussian energies (8 to 16 KJ/mol) and retention energies (<40 KJ/mol) values within the same range, suggesting complex physical and weak chemical mechanisms involving ion exchange processes. The retention of Zn (II) by CA as well as M.CA and L.CA exhibited endothermic and spontaneous properties.

Recommendation: The adsorption properties of calcite in multi-ions adsorption system, by considering the competitive effects of the present ions on the surface of calcite and the operated mechanism, will be evaluated in further detail studies.

References

1. Salam, M.A.; Mokhtar, M.; Albukhari, S.M.; Baamer, D.F.; Palmisano, L.; Jaremko, M.; Abukhadra, M.R. Synthesis and Characterization of Green ZnO@ polynaniline/Bentonite Tripartite Structure (G. Zn@ PN/BE) as Adsorbent for As (V) Ions: Integration, Steric, and Energetic Properties. *Polymers* **2022**, *14*, 2329. [CrossRef] [PubMed]
2. Yang, X.; Wang, J.; El-Sherbeeny, A.M.; AlHammadi, A.A.; Park, W.-H.; Abukhadra, M.R. Insight into the adsorption and oxidation activity of a ZnO/piezoelectric quartz core-shell for enhanced decontamination of ibuprofen: Steric, energetic, and oxidation studies. *Chem. Eng. J.* **2022**, *431*, 134312. [CrossRef]

3. Sayed, I.R.; Farhan, A.M.; AlHammadi, A.A.; El-Sayed, M.I.; El-Gaied, I.M.A.; El-Sherbeeny, A.M.; Al Zoubi, W.; Ko, Y.G.; Abukhadra, M.R. Synthesis of novel nanoporous zinc phosphate/hydroxyapatite nano-rods (ZPh/HPANRs) core/shell for enhanced adsorption of Ni^{2+} and Co^{2+} ions: Characterization and application. *J. Mol. Liq.* **2022**, *360*, 119527. [CrossRef]

4. Javaheri, F.; Kheshti, Z.; Ghasemi, S.; Altaee, A. Enhancement of Cd^{2+} removal from aqueous solution by multifunctional mesoporous silica: Equilibrium isotherms and kinetics study. *Sep. Purif. Technol.* **2019**, *224*, 199–208. [CrossRef]

5. Jiang, Y.; Abukhadra, M.R.; Refay, N.M.; Sharaf, M.F.; El-Meligy, M.A.; Awwad, E.M. Synthesis of chitosan/MCM-48 and β-cyclodextrin/MCM-48 composites as bio-adsorbents for environmental removal of Cd^{2+} ions; kinetic and equilibrium studies. *React. Funct. Polym.* **2020**, *154*, 104675. [CrossRef]

6. Igiri, B.E.; Okoduwa, S.I.; Idoko, G.O.; Akabuogu, E.P.; Adeyi, A.O.; Ejiogu, I.K. Toxicity and Bioremediation of Heavy Metals Contaminated Ecosystem from Tannery Wastewater: A Review. *J. Toxicol.* **2018**, *2018*, 2568038. [CrossRef]

7. Samieifard, R.; Landi, A.; Pourreza, N. Adsorption of Cd, Co and Zn from multi-ionic solutions onto Iranian sepiolite isotherms. *Cent. Asian J. Environ. Sci. Technol. Innov.* **2021**, *2*, 102–118.

8. Pan, J.; Gao, B.; Guo, K.; Gao, Y.; Xu, X.; Yue, Q. Insights into selective adsorption mechanism of copper and zinc ions onto biogas residue-based adsorbent: Theoretical calculation and electronegativity difference. *Sci. Total Environ.* **2022**, *805*, 150413. [CrossRef]

9. Wu, K.; Meng, Y.; Gong, Y.; Wu, L.; Liu, W.; Ding, X. Drinking water elements constituent profiles and health risk assessment in Wuxi, China. *Environ. Monit. Assess.* **2022**, *194*, 1–13. [CrossRef]

10. Zhu, Z.; Wu, Y.; Hu, C.; Zhang, L.; Ding, H.; Zhu, Y.; Fan, Y.; Deng, H.; Zhou, X.; Tang, S. Elimination of zinc ions from aqueous solution by a hydroxylapatite-biochar composite material with the hierarchical porous microstructures of sugarcane waste. *J. Clean. Prod.* **2022**, *362*, 132483. [CrossRef]

11. O'Connor, K.F.; Al-Abed, S.R.; Hordern, S.; Pinto, P.X. Assessing the efficiency and mechanism of zinc adsorption onto biochars from poultry litter and softwood feedstocks. *Bioresour. Technol. Rep.* **2022**, *18*, 101039. [CrossRef] [PubMed]

12. Chowdhury, S.; Mazumder, M.J.; Al-Attas, O.; Husain, T. Heavy metals in drinking water: Occurrences, implications, and future needs in developing countries. *Sci. Total Environ.* **2016**, *569–570*, 476–488. [CrossRef] [PubMed]

13. Tadesse, S.H. Application of Ethiopian bentonite for water treatment containing zinc. *Emerg. Contam.* **2022**, *8*, 113–122. [CrossRef]

14. Cherono, F.; Mburu, N.; Kakoi, B. Adsorption of lead, copper and zinc in a multi-metal aqueous solution by waste rubber tires for the design of single batch adsorber. *Heliyon* **2021**, *7*, e08254. [CrossRef] [PubMed]

15. Ofudje, E.A.; Adedapo, A.E.; Oladeji, O.B.; Sodiya, E.F.; Ibadin, F.H.; Zhang, D. Nano-rod hydroxyapatite for the uptake of nickel ions: Effect of sintering behaviour on adsorption parameters. *J. Environ. Chem. Eng.* **2021**, *9*, 105931. [CrossRef]

16. El-Sherbeeny, A.M.; Ibrahim, S.M.; AlHammadi, A.A.; Soliman, A.T.A.; Shim, J.-J.; Abukhadra, M.R. Effective retention of radioactive Cs+ and Ba^{2+} ions using β-cyclodextrin functionalized diatomite (β-CD/D) as environmental adsorbent; characterization, application, and safety. *Surf. Interfaces* **2021**, *26*, 101434. [CrossRef]

17. Kadeche, A.; Ramdani, A.; Adjdir, M.; Guendouzi, A.; Taleb, S.; Kaid, M.; Deratani, A. Preparation, characterization and application of Fe-pillared bentonite to the removal of Coomassie blue dye from aqueous solutions. *Res. Chem. Intermed.* **2020**, *46*, 4985–5008. [CrossRef]

18. Chen, Y.; Nie, Z.; Gao, J.; Wang, J.; Cai, M. A novel adsorbent of bentonite modified chitosan-microcrystalline cellulose aerogel prepared by bidirectional regeneration strategy for Pb(II) removal. *J. Environ. Chem. Eng.* **2021**, *9*, 105755. [CrossRef]

19. Albukhari, S.M.; Salam, M.A.; Abukhadra, M.R. Effective retention of inorganic Selenium ions (Se (VI) and Se (IV)) using novel sodalite structures from muscovite; characterization and mechanism. *J. Taiwan Inst. Chem. Eng.* **2021**, *120*, 116–126. [CrossRef]

20. Wang, J.; Zhao, J.; Qiao, Y.; Luan, Z. Effect of Mg (II), Mn (II), and Fe (II) doping on the mechanical properties and electronic structure of calcite. *Mater. Today Commun.* **2022**, *2022*, 103725. [CrossRef]

21. Raju, C.; Anitha, J.; Kalyani, R.M.; Satyanandam, K.; Jagadeesh, P. Sorption of cobalt using marine macro seaweed graciliariacorti-catared algae powder. *Mater. Today Proc.* **2021**, *44*, 1816–1827. [CrossRef]

22. Bin Jumah, M.N.; Eid, M.H.; Al-Huqail, A.A.; Mohammad, M.A.; Bin-Murdhi, N.S.; Abu-Taweel, G.M.; Altoom, N.; Allam, A.A.; AbuKhadra, M.R. Enhanced remediation of As (V) and Hg (II) ions from aqueous environments using β-cyclodextrin/MCM-48 composite: Batch and column studies. *J. Water Process. Eng.* **2021**, *42*, 102118. [CrossRef]

23. Vieira, Y.; Netto, M.S.; Lima, É.C.; Anastopoulos, I.; Oliveira, M.L.; Dotto, G.L. An overview of geological originated materials as a trend for adsorption in wastewater treatment. *Geosci. Front.* **2022**, *101150*, 101150. [CrossRef]

24. Luo, C.; Yang, X.; Li, J. Mechanical Properties of Single-Crystal Calcite and Their Temperature and Strain-Rate Effects. *Materials* **2022**, *15*, 4613. [CrossRef]

25. Sabry, M.; Alazab, H.A.; Gad, A.; El-Faramawy, N. Thermoluminescence properties of natural Egyptian calcite. *J. Lumin.* **2021**, *238*, 118273. [CrossRef]

26. Carchini, G.; Hussein, I.; Al-Marri, M.J.; Shawabkeh, R.; Mahmoud, M.; Aparicio, S. A theoretical study of gas adsorption on calcite for CO_2 enhanced natural gas recovery. *Appl. Surf. Sci.* **2020**, *504*, 144575. [CrossRef]

27. Gunasekaran, S.; Anbalagan, G. Spectroscopic characterization of natural calcite minerals. *Spectrochim. Acta Part A Mol. Biomol. Spectrosc.* **2001**, *68*, 656–664. [CrossRef]

28. Tangarfa, M.; Hassani, N.S.A.; Alaoui, A. Behavior and Mechanism of Tannic Acid Adsorption on the Calcite Surface: Isothermal, Kinetic, and Thermodynamic Studies. *ACS Omega* **2019**, *4*, 19647–19654. [CrossRef]

29. Ban, M.; Luxbacher, T.; Lützenkirchen, J.; Viani, A.; Bianchi, S.; Hradil, K.; Rohatsch, A.; Castelvetro, V. Evolution of calcite surfaces upon thermal decomposition, characterized by electrokinetics, in-situ XRD, and SEM. *Colloids Surf. A Physicochem. Eng. Asp.* **2021**, *624*, 126761. [CrossRef]

30. Ulian, G.; Moro, D.; Valdrè, G. Elastic properties of heterodesmic composite structures: The case of calcite $CaCO_3$ (space group R3̄c). *Compos. Part C Open Access* **2021**, *6*, 100184. [CrossRef]

31. Vivas, E.L.; Cho, K. Efficient adsorptive removal of Cobalt(II) ions from water by dicalcium phosphate dihydrate. *J. Environ. Manag.* **2021**, *283*, 111990. [CrossRef] [PubMed]

32. Abukhadra, M.R.; AlHammadi, A.A.; Khim, J.S.; Ajarem, J.S.; Allam, A.A. Enhanced decontamination of Levofloxacin residuals from water using recycled glass based a green zinc oxide/mesoporous silica nanocomposite; adsorption and advanced oxidation studies. *J. Clean. Prod.* **2022**, *356*, 131836. [CrossRef]

33. Yuan, M.; Gu, Z.; Xia, S.; Zhao, J.; Wang, X. In-situ remediation of zinc contaminated soil using phosphorus recovery product: Hydroxyapatite/calcium silicate hydrate (HAP/C–S–H). *Chemosphere* **2021**, *286*, 131664. [CrossRef] [PubMed]

34. El Qada, E. Kinetic Behavior of the Adsorption of Malachite Green Using Jordanian Diatomite as Adsorbent. *Jordanian J. Eng. Chem. Ind. (JJECI) Res. Pap.* **2020**, *3*, 1–10. [CrossRef]

35. Salam, M.A.; Abukhadra, M.R.; Mostafa, M. Effective decontamination of As (V), Hg (II), and U (VI) toxic ions from water using novel muscovite/zeolite aluminosilicate composite: Adsorption behavior and mechanism. *Environ. Sci. Pollut. Res.* **2020**, *27*, 13247–13260. [CrossRef]

36. Lin, X.; Xie, Y.; Lu, H.; Xin, Y.; Altaf, R.; Zhu, S.; Liu, D. Facile preparation of dual La-Zr modified magnetite adsorbents for efficient and selective phosphorus recovery. *Chem. Eng. J.* **2021**, *413*, 127530. [CrossRef]

37. Huang, Y.; Li, S.; Chen, J.; Zhang, X.; Chen, Y. Adsorption of Pb (II) on mesoporous activated carbons fabricated from water hyacinth using H3PO4 activation: Adsorption capacity, kinetic and isotherm studies. *Appl. Surf. Sci.* **2014**, *293*, 160–168. [CrossRef]

38. Sherlala, A.; Raman, A.; Bello, M.; Buthiyappan, A. Adsorption of arsenic using chitosan magnetic graphene oxide nanocomposite. *J. Environ. Manag.* **2019**, *246*, 547–556. [CrossRef]

39. Huang, Y.; Zeng, X.; Guo, L.; Lan, J.; Zhang, L.; Cao, D. Heavy metal ion removal of wastewater by zeolite-imidazolate frameworks. *Sep. Purif. Technol.* **2018**, *194*, 462–469. [CrossRef]

40. Jasper, E.E.; Ajibola, V.O.; Onwuka, J.C. Nonlinear regression analysis of the sorption of crystal violet and methylene blue from aqueous solutions onto an agro-waste derived activated carbon. *Appl. Water Sci.* **2020**, *10*, 1–11. [CrossRef]

41. Ashraf, M.-T.; AlHammadi, A.A.; El-Sherbeeny, A.M.; Alhammadi, S.; Al Zoubi, W.; Ko, Y.G.; Abukhadra, M.R. Synthesis of cellulose fibers/Zeolite-A nanocomposite as an environmental adsorbent for organic and inorganic selenium ions; Characterization and advanced equilibrium studies. *J. Mol. Liq.* **2022**, *360*, 119573. [CrossRef]

42. Giles, C.H.; MacEwan, T.H.; Nakhwa, S.N.; Smith, D. Studies in adsorption. Part XI. A system of classification of solution adsorption isotherms, and its use in diagnosis of adsorption mechanisms and in measurement of specific surface areas of solids. *J. Chem. Soc.* **1960**, *111*, 3973–3993. [CrossRef]

43. Abukhadra, M.R.; Dardir, F.M.; Shaban, M.; Ahmed, E.A.; Soliman, M.F. Superior removal of Co^{2+}, Cu^{2+} and Zn^{2+} contaminants from water utilizing spongy Ni/Fe carbonate–fluorapatite; preparation, application and mechanism. *Ecotoxicol. Environ. Saf.* **2018**, *157*, 358–368. [CrossRef] [PubMed]

44. Shaban, M.; Abukhadra, M.R.; Shahien, M.G.; Khan, A.A.P. Upgraded modified forms of bituminous coal for the removal of safranin-T dye from aqueous solution. *Environ. Sci. Pollut. Res.* **2017**, *24*, 18135–18151. [CrossRef]

45. Dawodu, F.; Akpomie, G.; Abuh, M. Equilibrium Isotherm Studies on the Batch Sorption of Copper (II) ions from Aqueous Solution unto Nsu Clay. *Int. J. Sci. Eng. Res.* **2012**, *3*, 1–7.

46. Mobarak, M.; Ali, R.A.; Seliem, M.K. Chitosan/activated coal composite as an effective adsorbent for Mn(VII): Modeling and interpretation of physicochemical parameters. *Int. J. Biol. Macromol.* **2021**, *186*, 750–758. [CrossRef]

47. Hua, P.; Sellaoui, L.; Franco, D.; Netto, M.S.; Dotto, G.L.; Bajahzar, A.; Belmabrouk, H.; Bonilla-Petriciolet, A.; Li, Z. Adsorption of acid green and procion red on a magnetic geopolymer based adsorbent: Experiments, characterization and theoretical treatment. *Chem. Eng. J.* **2020**, *383*, 123113. [CrossRef]

48. Dhaouadi, F.; Sellaoui, L.; Reynel-Ávila, H.E.; Landín-Sandoval, V.; Mendoza-Castillo, D.I.; Jaime-Leal, J.E.; Lima, E.C.; Bonilla-Petriciolet, A.; Lamine, A.B. Adsorption mechanism of Zn^{2+}, Ni^{2+}, Cd^{2+}, and Cu^{2+} ions by carbon-based adsorbents: Interpretation of the adsorption isotherms via physical modelling. *Environ. Sci. Pollut. Res.* **2021**, *28*, 30943–30954. [CrossRef]

49. Sellaoui, L.; Ali, J.; Badawi, M.; Bonilla-Petriciolet, A.; Chen, Z. Understanding the adsorption mechanism of Ag+ and Hg^{2+} on functionalized layered double hydroxide via statistical physics modeling. *Appl. Clay Sci.* **2020**, *198*, 105828. [CrossRef]

50. Lacombe, O. Calcite Deformation Twins: From Crystal Plasticity to Applications in Geosciences. *Geosciences* **2022**, *12*, 280. [CrossRef]

51. Dhaouadi, F.; Sellaoui, L.; Badawi, M.; Reynel-Ávila, H.E.; Mendoza-Castillo, D.I.; Jaime-Leal, J.E.; Bonilla-Petriciolet, A.; Ben Lamine, A. Statistical physics interpretation of the adsorption mechanism of Pb^{2+}, Cd^{2+} and Ni^{2+} on chicken feathers. *J. Mol. Liq.* **2020**, *319*, 114168. [CrossRef]

52. Sellaoui, L.; Guedidi, H.; SarraWjihi, S.; Reinert, L.; Knani, S.; Duclaux, L.; Ben Lamine, A. Experimental and theoretical studies of adsorption of ibuprofen on raw and two chemically modified activated carbons: New physicochemical interpretations. *RSC Adv.* **2016**, *6*, 12363–12373. [CrossRef]

53. Yue, H.; Shang, Z.; Xu, P.; Feng, D.; Li, X. Preparation of EDTA modified chitooligosaccharide/sodium alginate/Ca^{2+} physical double network hydrogel by using of high-salinity oilfield produced water for adsorption of Zn^{2+}, Ni^{2+} and Mn^{2+}. *Sep. Purif. Technol.* **2022**, *280*, 119767. [CrossRef]

54. Abukhadra, M.R.; Bakry, B.M.; Adlii, A.; Yakout, S.M.; El-Zaidy, M.E. Facile conversion of kaolinite into clay nanotubes (KNTs) of enhanced adsorption properties for toxic heavy metals (Zn^{2+}, Cd^{2+}, Pb^{2+}, and Cr^{6+}) from water. *J. Hazard. Mater.* **2019**, *374*, 296–308. [CrossRef]

55. Biswas, S.; Bal, M.; Behera, S.K.; Sen, T.K.; Meikap, B.C. Process Optimization Study of Zn^{2+} Adsorption on Biochar-Alginate Composite Adsorbent by Response Surface Methodology (RSM). *Water* **2019**, *11*, 325. [CrossRef]

56. Bao, S.; Tang, L.; Li, K.; Ning, P.; Peng, J.; Guo, H.; Zhu, T.; Liu, Y. Highly selective removal of Zn(II) ion from hot-dip galvanizing pickling waste with amino-functionalized Fe$_3$O$_4$@SiO$_2$ magnetic nano-adsorbent. *J. Colloid Interface Sci.* **2016**, *462*, 235–242. [CrossRef]

57. Tian, W.; Rong, Y.; Li, D.; Tian, J.; Lin, N.; Wang, Z. Self-templated formation and characterization of polyhedral CoS hollow nanocage (HNC) for heavy metal ions (Ag+, Cd^{2+}, Cu^{2+}, Pb^{2+} and Zn^{2+}) removal in aqueous solutions. *J. Phys. Chem. Solids* **2022**, *162*, 110516. [CrossRef]

58. Zhou, C.; Wang, X.; Wang, Y.; Song, X.; Fang, D.; Ge, S. The sorption of single- and multi-heavy metals in aqueous solution using enhanced nano-hydroxyapatite assisted with ultrasonic. *J. Environ. Chem. Eng.* **2021**, *9*, 105240. [CrossRef]

59. Ni, P.; Fox, J.T. Synthesis and appraisal of a hydroxyapatite/pectin hybrid material for zinc removal from water. *RSC Adv.* **2019**, *9*, 21095–21105. [CrossRef]

60. Li, Z.; Gong, Y.; Zhao, D.; Dang, Z.; Lin, Z. Enhanced removal of zinc and cadmium from water using carboxymethyl cellulose-bridged chlorapatite nanoparticles. *Chemosphere* **2021**, *263*, 128038. [CrossRef]